A Statistical Model for the Error Bounds of an Active Phased Array Antenna for SAR Applications

Paul Snoeij and Arjen R. Vellekoop

Abstract—**Radiometric calibration of a SAR-image is achieved by monitoring all the relevant parameters of the radar equation. The precision and accuracy of the instrument are limited by the errors made in monitoring these parameters. Whereas most parameters can quite readily and constantly be monitored, monitoring of the array pattern during the flight is a cumbersome and time-consuming affair, and, therefore, mostly omitted. Random variations in the antenna pattern can thus be expected to have the greatest influence on the uncertainty of the scatter-coefficient estimate. Obviously, the effect of a phased array antenna, of which the antenna pattern is formed by the amplitude and phase of several individual T/R-modules fed to radiating elements, will be even worse. This paper reviews a model for the theoretical error bounds for the radiometric calibration of SAR imagery. The model is then applied utilizing the radar system parameters as will be used in the project PHARUS (acronym for PHased ARray Universal Sar) [1], a Dutch polarimetric airborne *C*-band universal SAR, which is currently under construction. An error model for the phased array antenna pattern will be presented. This model was applied to a 16x8 phased array antenna to determine the influence of errors in the T/R modules and angle variations of the beam direction.**

I. Introduction

THE advantages of the phased array antenna which are generally not encountered in other antenna types has lead to an increased interest in its application in remote sensing radar systems. Both beam direction and gain pattern can electronically be controlled. The possibility of shaping the gain pattern has positive effect on sidelobe levels. The flexibility offered by a phased array system, however, has a few drawbacks: Besides the higher cost, the system needs more complex circuitry, and often requires computer control, especially when electronic beam control is implemented. Full testing of a phased array is a cumbersome affair. Since the phase and amplitude of the elements of the phased array are controlled by several phase shifters and power amplifiers, the synthesized gain pattern in particular will become a part of the system. Environmental influences and aging of the electronics will yield directly to a degradation of the antenna gain pattern. Considering the random nature of variations of electronic circuitry, the excitation coefficients of the antenna array will show random perturbations as well, leading to a random degraded gain pattern.

Manuscript received September 16, 1991; revised February 25, 1992. This work was supported by the Ministry of Defense and by the Netherlands Remote Sensing Board (BCRS).

The authors are with the Delft University of Technology, Laboratory for Telecommunication and Remote Sensing Technology, 2600 GA Delft, The Netherlands.

IEEE Log Number 9200973.

In the case of a digital system, in which the phase and amplitude of each of the T/R-modules of the radar antenna-array have a discrete set of values, the desired aperture illumination will show quantization errors. The minimization of these errors obviously needs a large number of discrete values. However, in an airborne radar such as SLAR or SAR the beam direction can only be stabilized to a certain extent and also will show a random (measurement) error. The number of discrete values, or number of bits, required for the amplitude and phase settings, can now be determined by taking the maximum possible quantization error smaller than the beam direction error.

In Section II of this paper we discuss the calibration aspects in remote sensing radars. In Section III the error model given in [2] was used the determine the system parameter error which has the most important influence on the SAR calibration. In Section IV the phased array antenna pattern will be discussed while in Section V we present a model to calculate the theoretical error bounds on the phased array gain pattern based upon a statistical coefficient of variation model [2], [3]. As an example, the model is then applied in Section VI to a 16x8 phased array antenna to determine the influence of random amplitude and phase fluctuations of the individual T/R-modules feeding the radiating elements, as well as random angle variations of the beam-direction. The relevance of the model regarding the amplitude and phase variations is tested by comparing the results with the exact solution as described by Zaghloul [4]. Even for large variations the model is in good agreement with the exact solution. The calculation effort of the model, however, is very much smaller than the required calculation effort of the exact solution.

II. Calibration Aspects

Like the majority of measurements in physics, remote sensing belongs to the class of so-called indirect measurements. An important characteristic of such indirect measurements is that always a graduated scale is needed to reduce the quantity to be measured to the one that is actually measured and *de facto* the creation of such a scale is the objective of calibration.

In order to systematize this discussion on calibration aspects it is helpful to model the radar observation process by means of a layered structure (Fig. 1.). At the lowest level we start with the object layer. This layer may contain one of the well-known object classes and it is assumed that one wants to study the impact of the "physical world" on that particular class. The layer next to the object layer is the electromagnetic interaction layer, at this very level the radar-echo is formed which starts

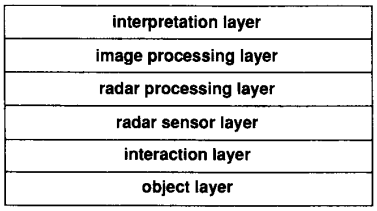

Fig. 1. The layered structure of the radar observation process.

the observation process. The sensor layer, which comes next, represents the actual measurement of σ as a power ratio. In many cases, the radar signal still needs some processing, which is performed in the fourth layer. In its simplest form this processing will only take care of the quantization and subsequent digitization of the power ratio, to make it ready for presentation. In the case of an advanced system like a SAR the processing will be part of the actual measurement of the power ratio. Usually, the system output will be made available as an image in digital format, to be further processed by the user (layer 5). In most cases, the top layer is the (human) interpretation layer where the observation process is concluded.

Having introduced the layered observation structure the calibration problem may be analyzed in more detail. In this context it is interesting to note that the layered structure approach strongly suggests that calibration may be performed at different levels.

Obviously, the most comprehensive form of radar calibration in remote sensing will be obtained when a graduated σ-scale at the interpretation level is calibrated in terms of the object parameter to be measured. This may be called a physical calibration. Although physical calibration may seem to be the optimum, since it includes all layers, it will not be feasible in practice. One major reason is that it is impossible to repeat such calibrations frequently enough and, consequently, the instrument would have to be perfectly stable. Another reason is that the required radar signal processing in general can only be performed off-line, which is an unfavorable situation for physical calibration.

A more practical approach to the calibration is usually obtained by dividing the observation structure into a number of substructures. Following this idea it makes sense to combine the lower two layers to form the first substructure. At this level calibration includes the determination of object signatures, i.e., the measurement of their radar "behavior" as a function of as many parameters as possible. Measurements of this kind are characterized as basic and they are performed by scatterometers, either groundbased or airborne. By means of such measurements we have learned a lot about the nature of the radar-echo's as they are produced by remote sensing objects.

Assuming that the object signatures are known, the calibration problem is reduced to a calibration of the sensor in terms of power relations which seems a technical rather then a physical problem. In this way, the radar becomes a measuring instrument in the usual sense, whether this instrument will combine the sensor (layer 3) and processing (layer 4) functions or not, depends on the type of system.

A good measuring instrument must be accurate, precise and stable. "Accurate" implies "conforming to truth," "precise" means "well defined" whereas an instrument is said to be stable if repetition of the same measurement yields the same reading. Precision and stability are design objectives, while accuracy is a matter of calibration. This statement is in no way trivial: Too many people are thinking that the quality of an instrument may be improved by frequent calibration. With an instrument that fulfills the accuracy, precision and stability requirements the image processing can be based on true σ-values. Needless to say, procedures like filtering, which potentially may interfere with the "truth-principle," have to be applied with great care. Finally, at the interpretation level, the σ-values will have to be combined with the signature data to yield information on the object.

The assumption that the calibration of the radar may be based on power measurements alone is actually an oversimplification. This is caused by the fact that, in remote sensing, the radar is collecting the power scattered by a certain area or volume, the resolution cell. The usual assumption is then that the radar return of each resolution cell can be replaced by that of a distribution of N-point scatterers. Under certain conditions, the radiation of these N scatterers can be added on an incoherent or power basis. Since each point target is seen from the radar location in a different direction, however, the power contribution of each individual point scatterer has to be weighted according to the magnitude of the antenna pattern in the direction that applies. Therefore, it turns out that the antenna gain and the antenna pattern are of equal importance.

The ultimate consequence of this power-addition requirement would be a preference for, straight-on, system designs based on the application of, e.g., passive antennas. For such systems the calibration problem may be divided in two parts: The external calibration takes care of the antenna pattern, including the antenna gain, whereas the power relation in the transmitter–receiver chain is calibrated by an internal loop.

In case of an advanced SAR-system based on the use of a distributed phased array antenna both calibrations will mix and the internal calibration, in particular, will become a fiction. Active antennas like this can only be calibrated when they are operational, i.e., when all transmitter and receiver modules are active. In fact, also in this case one would prefer a system that is as simple as possible since each operational mode (like incidence angle, swath-width, or polarization) will ask for an additional calibration. In general, two options can be considered appropriate for the calibration of active antennas: The use of a homogeneous distributed target, of which the scatter coefficient is known, or the use of a point target of known cross-section in combination with antenna pattern measurements for all operational modes and a monitoring of the amplitude and phase behavior of all transmitter–receiver modules.

Needless to say, the system stability must be good enough to bridge the time period between two calibrations. In the meantime, in fact, only the appropriate functioning of the array components can be supervised. The outcome of this bookkeeping could be incorporated in the signal processing.

TABLE I
NOMENCLATURE OF VARIABLES AFTER [2]

λ	radar wavelength
i	subscript: scene to be calibrated
r	subscript: reference target scene
A	received amplitude
A_n	amplitude of the additive SAR system noise
θ	radar incidence angle
M	multiplicative noise ratio
$\hat{a}m$ or αm	multiplicative calibration offset factor
Pav	average transmitted power
ra	azimuth resolution
rs	slant range resolution
R	slant range
G	antenna gain function
H	square of the total SAR system gain term
u	platform velocity

III. ERROR BOUNDS IN THE RADIOMETRIC CALIBRATION OF PHARUS

The error model used is based upon the Coefficient of Variation Error Model [2]. The (fractional) coefficient of variation is defined after [2] as

$$\epsilon_x = \frac{s_x}{< X >} \tag{1}$$

with s_x the sample standard deviation and <X> the average value of a random distributed variable X. The coefficient of variation ϵ is assumed to include both natural as well as measurement error variability.

In this paper we use the same nomenclature for the variables as in [2] (Table I) and using (24), (26), and (27) from [2] the coefficients of variation in the case of absolute calibration $\varepsilon_{\sigma a}$, relative absolute comparison $\varepsilon_{\sigma ra}$, relative interscene calibration $\varepsilon_{\sigma rb}$, and relative intrascene calibration $\varepsilon_{\sigma rw}$ can be determined. The conversion to dB values used in this paper is based on (27) [2].

A. PHARUS System Parameter Errors

To apply the error model to the PHARUS-system the different coefficients of variation has to be defined. In Table II the values of the errors are summarized. For a number of these coefficients values had to be assumed because the system was still in its definition phase; after the construction of the system, the real values can be used. During the definition phase of the PHARUS project a number of design goals were specified. For example, the phased array antenna would consist of 128 individual T/R modules, each using a separate patch antenna, resulting in a transmitted power of 128*20 = 2560 W. The operational altitude of the system was assumed to be 6 km, and the incidence angle would range from 20↔85°. At the end of the calibration study, however, the design goals were adjusted due to financial restrictions. The calculations given in this paper are still based on the initial design.

The error in the incidence angle $\epsilon_{\sin\theta}$ can be determined from the errors in the altitude h and slant range R, and is dependent on those errors. The coefficient of variation for the incidence angle is given by

$$\epsilon_{\sin\theta} = \sqrt{\left(\frac{\partial \sin\theta}{\partial h}\Delta h + \frac{\partial \sin\theta}{\partial R}\Delta R\right)^2}\ \frac{1}{\sin\theta} = \frac{1}{\tan^2\theta}\sqrt{\epsilon_h^2 + \epsilon_R^2}. \tag{2}$$

The measurement error in altitude and slant range has been estimated on 15 m. In the worst case (incidence angle θ=20°) the error in the incidence angle is, with h = 6 km and R = 6385 m, $\varepsilon_{\sin\theta}$ = 0.0259.

The total additive noise figure for the PHARUS system is estimated on 10 dB or HA_n^2 = 10. The maximum possible multiplicative noise ratio is estimated on 13 dB, or M = 0.05. We assume that the error in M is ϵ_M = 0.1.

TABLE II
PHARUS SYSTEM PARAMETERS AND ERROR MODEL VALUES

Parameter	Range of Values	Nominal Value
Frequency	•	5.3 GHz
Wavelength	•	5.66 cm
Transmitter Power (peak)	•	2560 W
Pulsewidth	•	10 μs
PRF	1000–4000	2500 Hz
Receiver Noise Figure	•	3 dB
System losses	•	6 dB
ϵ_{Ai}	•	.05
ϵ_{Ani}	•	.05
ϵ_{Ar}	•	.05
ϵ_{Anr}	•	.05
$\epsilon_{\sin\theta i}$	.0259–1.92·10^{-5}	.00209
$\epsilon_{\sin\theta r}$	.0259–1.92·10^{-5}	.00209
ϵ_{Mi}	•	.10
ϵ_{Mr}	•	.10
$\epsilon_{\hat{a}m}$	.05–.50	.20
ϵ_{Pavi}	•	.05
ϵ_{Pavr}	•	.05
ϵ_{ra}	•	.05
ϵ_{rs}	•	.05
ϵ_{Ri}	.00235–2.18·10^{-4}	.0016
ϵ_{Rr}	.00235–2.18·10^{-4}	.0016
ϵ_{Gi}	0–.20	.10
ϵ_{Gr}	0–.20	.10
ϵ_{Hi}	•	.05
ϵ_{Hr}	•	.05
ϵ_{ui}	•	.004
ϵ_{ur}	•	.004

B. PHARUS System Error Analysis

With the nominal values given in Table II the different nominal errors of the SAR-instrument can be calculated. The worst case situation exists with the smallest incidence angle θ = 20° and ϵ_G = 0.2 (Table III). The contributions of the errors as a percentage of the values given in Table III for the relative interscene calibration are given in Fig. 2 while in

TABLE III
NOMINAL AND WORST CASE ERROR BOUNDS

		Nominal	Worst case
Absolute error bound	s_a	1.617 dB	2.610 dB
Relative absolute error bound	s_{ra}	2.520 dB	4.314 dB
Relative interscene error bound	s_{rb}	1.786 dB	3.661 dB
Relative intrascene error bound	s_{rw}	1.698 dB	3.587 dB

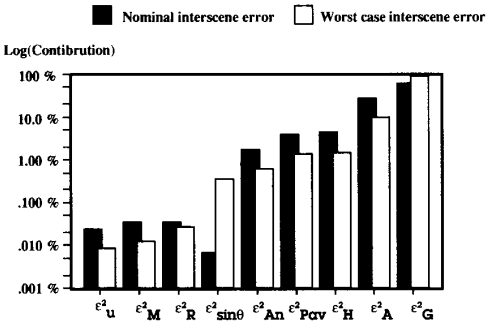

Fig. 2. Contribution of the different errors in the relative interscene calibration (logarithmic scale in percentages).

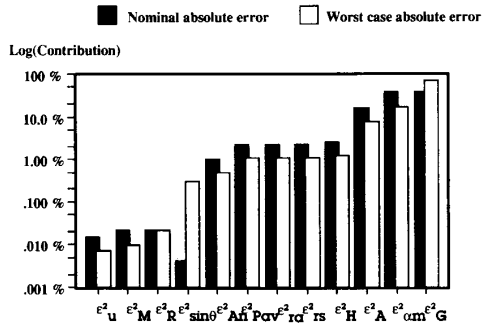

Fig. 3. Contribution of the different errors in the relative absolute calibration (logarithmic scale in percentages).

Fig. 3 the contributions to the relative absolute calibration are shown.

From applying the error model using the PHARUS design parameters the following conclusions can be made:

1. The error in the gain ϵ_G has the largest influence on the overall error. Minimizing this variable has the highest priority in the system design.
2. The single error terms (e.g., ϵ_u, ϵ_{ra}) show a small influence on the accuracy. Errors of less then 20% can still be accepted.
3. The quadratic terms and third power term ϵ_R needs to be looked after. The error in the received amplitude ϵ_A has the largest influence.

In the next sections the phased array antenna will be introduced and an error model will be presented which predicts the levels of uncertainty in the antenna gain due to random variations in amplitude and phase of the T/R modules as well as random angle variations.

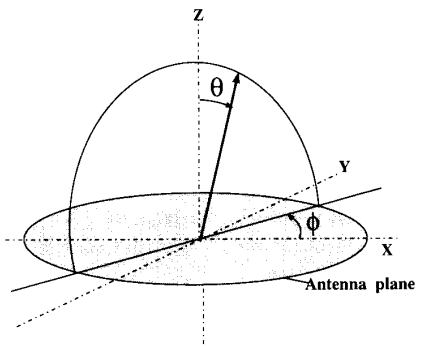

Fig. 4. Coordinate system for the planar phased array antenna with $z_{m,i} = 0$.

IV. PHASED ARRAY ANTENNA PATTERN

The far field $E(\theta, \phi)$ of an array of radiating elements fed by N T/R-modules each feeding M antenna elements can be expressed as

$$E(\theta, \phi) = \sum_{i=1}^{N} A_i e^{j\beta_i} \cdot F_i. \tag{3}$$

In which A_i and β_i are the amplitude and phase of the ith T/R-module, respectively, and F_i is the array function described as:

$$F_i = \sum_{m=1}^{M_i} c_{m,i} e^{j(ux_{m,i} + vy_{m,i} + wz_{m,i})} \cdot E_{m,i}(\theta, \phi) \tag{4}$$

with

M_i	number of elements fed by the ith T/R-module
$c_{m,i}$	complex excitation coefficient of the mth element fed by the ith T/R module
$x_{m,i}, y_{m,i}, z_{m,i}$	coordinates of the mth element fed by the ith T/R-module
u	$k\sin\theta\cos\phi$
v	$k\sin\theta\sin\phi$
w	$k\cos\theta$
k	the wavenumber $k = 2\pi/\lambda$
$E_{m,i}(\theta, \phi)$	gain pattern of the individual element

The gain pattern is proportional to the power density $S(\theta, \phi)$ which itself is proportional to the square magnitude of $E(\theta, \phi)$. The power density then follows as:

$$S(\theta, \phi) = \frac{1}{240\pi} \sum_{i=1}^{N} \sum_{n=1}^{N} A_i A_n e^{j(\beta_i - \beta_n)} F_i F_n^* \tag{5}$$

in which * denotes the complex conjugate.

Fig. 4 shows the coordinate system for a planar phased array antenna with $z_{m,i} = 0$.

To come to an expression of the exact influence of random amplitude, phase and angle perturbations, the integration of

the product of the probability distributions and the square of the power density function has to be calculated. Although the problem is in principle analytically solvable [4], the expression becomes a mathematical monster containing products of four series each with dimension *N*x*M*.

A more elegant approach to the probabilistic analysis can be found in an approximating solution. The approximating analysis will give more insight, and requires a far less computer effort than the exact solution. This approach will be discussed in the following section.

V. Gain Pattern Error Model

Let a population Y with mean μ_y have a sample estimate of $<Y>$ and a sample standard deviation σ_y , including population variability as well as measurement errors. The coefficient of variation then follows as:

$$\epsilon_y = \frac{\sigma_y}{< Y >}. \tag{6}$$

If the population can be described as a function of N random variables $Y = f(X_1, X_2, ..., X_n)$ with mean $X_i = \{\mu_1, \mu_2, ..., \mu_n\}$, the population can be represented by its first-order Taylor series expansion about the point $\mu_1, \mu_2, ..., \mu_n$:

$$Y \simeq a_0 + \sum_{i=1}^{N} a_i (X_i - \mu_i) \tag{7}$$

with

$$a_o = f(\mu_1, \mu_2, ..., \mu_n) \tag{8}$$

and

$$a_i = \frac{\partial f}{\partial X_i}(\mu_1, \mu_2, ..., \mu_n). \tag{9}$$

If the X_i's are independent (neglecting mutual coupling between the radiators) the mean and variance of the population then follow as:

$$\mu_y \simeq a_0 \tag{10}$$

$$\sigma_y^2 \simeq \sum_{i=1}^{N} a_i^2 \sigma_i^2. \tag{11}$$

The power density function consists of four variables showing random fluctuations: The amplitude and phase of the T/R-modules fed to the antenna elements, and the beam-direction angles θ and ϕ. Utilizing (7)–(11) to approximate the mean and variance of this power density function yields:

$$\mu_S = S(\mu_\theta, \mu_\phi, \mu_{A_1}, ..., \mu_{A_n}, \mu_{\beta_1}, ..., \mu_{\beta_n}) \tag{12}$$

$$\sigma_S^2 = \left\{\frac{dS}{d\theta}\right\}^2 \sigma_\theta^2 + \left\{\frac{dS}{d\phi}\right\} \sigma_\phi^2 + \sum_{k=1}^{N} \left\{\frac{dS}{dA_k}\right\}^2 \sigma_A^2 + \sum_{k=1}^{N} \left\{\frac{dS}{d\beta_k}\right\}^2 \sigma_\beta^2 \Bigg| \{\mu_\theta, \mu_\phi, \mu_{A_1}, \mu_{A_2}, ..., \mu_{A_n}, \mu_{\beta_1}, \mu_{\beta_2}, ..., \mu_{\beta_n}\}. \tag{13}$$

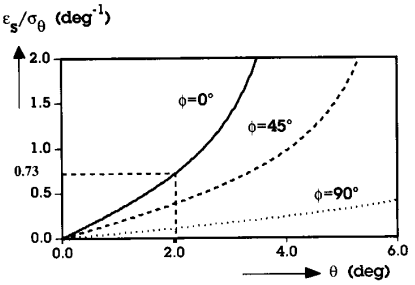

Fig. 5. The normalized variation-coefficient ϵ_s/σ_θ as a function of θ, with ϕ as parameter.

The coefficient of variation then follows as $\varepsilon_s = \sigma_s/\mu_s$.

VI. Example of a Phased Array Antenna

To explore the utility of the model a probabilistic analysis of a simple phased array antenna will be performed. The antenna consists of an array of 16×8 ideally radiating elements ($E_{m,i}(\theta, \phi) = 1$), each fed by a single T/R-module (*M*=1, *N*=128). The element distance in *x*-direction is Δx = 44 mm, in *y* direction Δy = 37 mm, leading to a physical dimension of 16*44 mm x 8*37 mm ≈0.7x0.3 m^2. The antenna is operating in *C*-band with a wavelength of λ = 5.66 cm. Each T/R-module feeds an element with a Gaussian distributed amplitude and phase with mean μ_{Ai} =1 and $\mu_{\beta i}$= 0 and variance $\sigma_A{}^2$, and $\sigma_\beta{}^2$, respectively. The measurement errors being made in the determination of the angles θ and ϕ under which the gain pattern is considered, are expected to be Gaussian distributed with variances $\sigma_\theta{}^2$ and $\sigma_\phi{}^2$, respectively.

To find the coefficient of variation ϵ_s of the power density function $S(\theta, \phi)$ the variance $\sigma_s{}^2$ has to be determined by solving the partial derivatives in (13). The partial derivative of the power density function to θ follows as:

$$\frac{\partial S}{\partial \theta} = \frac{\partial}{\partial \theta}\left\{\sum_i^N \sum_n^N A_i A_n F_i F_n^*\right\} \Bigg| \left\{\mu_\theta, \mu_\phi, \mu_a = 1, \mu_\beta = 0\right\}$$
$$= jk \cos\mu_\theta \sum_i^N \sum_n^N \Big\{(\mu_{x_i} - \mu_{x_n}) \cos\mu_\phi + (\mu_{y_i} - \mu_{y_n}) \sin\mu_\phi\Big\} \cdot F_i F_n^*. \tag{14}$$

Fig. 5 shows the coefficient of variation normalized to σ_θ as a function of θ, with ϕ as parameter.

As could be expected, the largest error is being encountered in the ϕ = 0 direction or *x*-axis direction, where the antenna pattern has the largest gradient. Of special interest is the error made at the half power beamwidth $\theta_{-3dB} = 0.443 \cdot \lambda/L = 2°$ (*L*= antenna length), which has a worst-case value of $\varepsilon_S/\sigma_\theta$ = 0.73 deg^{-1}.

The expression for $\partial S/\partial \phi$ is simply encountered by interchanging the sine and cosine terms in (14), and negating the first term under the summation.

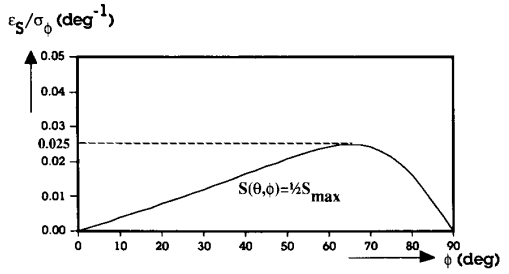

Fig. 6. The normalized variation-coefficient $\varepsilon_S/\sigma_\phi$ as a function of ϕ, with θ equal to the half power beamwidth.

$$\frac{dS}{d\phi} = \frac{d}{d\phi}\left\{\sum_i^N \sum_{j\neq i}^N A_i A_j e^{-j(\beta_i-\beta_j)} e^{jk\sin\theta\cos\phi\,(x_i-x_j)+jk\sin\theta\sin\phi\,(y_i-y_j)}\right\}$$

$$= jk\sin\theta \sum_i^N \sum_{j\neq i}^N A_i A_j \left\{-\sin\phi(x_i-x_j)+\cos\phi(y_i-y_j)\right\} e^{-j(\beta_i-\beta_j)} F_i F_j^*. \quad (15)$$

Fig. 6 shows the influence of ϕ on the variation-coefficient ε_S. The angle θ has been chosen equal to the half power beamwidth.

The next step is to determine the derivative of the power density function to the amplitude and phase per radiating element k:

$$\frac{\partial S}{\partial A_k} = \frac{\partial}{\partial A_k}\left\{\sum_{i=1}^N A_i A_k e^{-j(\beta_i-\beta_k)} F_i F_k^* + \sum_{i=1}^N A_k A_i e^{-j(\beta_k-\beta_i)} F_k F_i^*\right\} \Big| \left\{\mu_\theta, \mu_\phi, \mu_a = 1,\ \mu_\beta = 0\right\}$$

$$= 2\sum_{i=1}^N \cos\left(k\sin\mu_\theta\left\{(\mu_{x_k}-\mu_{x_i})\cos\mu_\phi + (\mu_{y_k}-\mu_{y_i})\sin\mu_\phi\right\}\right). \quad (16)$$

It is easily being verified that for $\theta = \phi = 0$ the outcome of (16) is $\partial S/\partial A = 2N$, so that the total contribution of N-elements to ${\sigma_S}^2$ will be $\sum\{2N\}^2 \cdot \sigma_A^2 = 4N^3\sigma_A^2$. With a mean power density of $\mu_S = N^2$ at $\theta = \phi = 0$, the contribution to the normalized coefficient of variation becomes $\varepsilon_S/\sigma_A = 2/\sqrt{N} = 0.177$ as can be seen in Fig 7.

Taking the derivative to the phase yields:

$$\frac{\partial S}{\partial \beta} = 2\sum_{i=1}^N \sin\left(k\sin\mu_\theta\left\{(\mu_{x_k}-\mu_{x_i})\cos\mu_\phi + (\mu_{y_k}-\mu_{y_i})\sin\mu_\phi\right\}\right). \quad (17)$$

The coefficient of variation normalized to both the amplitude and the phase is shown as a function of θ in Fig. 7 for ϕ=0.

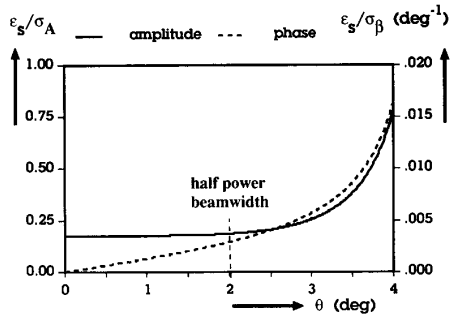

Fig. 7. Normalized coefficient of variation as a function of θ.

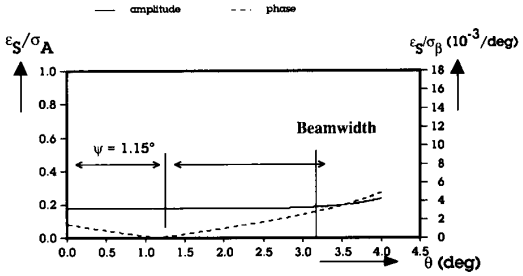

Fig. 8. The influence of the amplitude and phase variations on the normalized coefficient of variation as a function of the azimuth angle θ ($\phi = 0$). The antenna has a linear phase distribution in azimuth with $\beta_i = i{\cdot}5.625°$, resulting in an offset angle Ψ=1.15°.

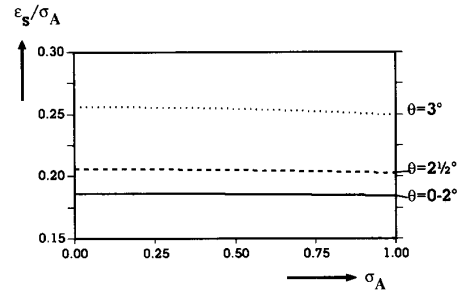

Fig. 9. The exact normalized coefficient of variation as a function of σ_A for ϕ = 0. There is hardly any change as σ_A increases.

The worst case situation is when the angle ϕ=0 en $\theta\approx2°$ (-3 dB points of the antenna pattern).

If the beam is switched ($\beta_k, \beta_i \neq 0$), the whole graph is shifting as can be seen in Fig. 8.

In Fig. 8 it is assumed that the phase is increasing linear with $\Delta\beta$=5.625°, which can be realized with a 6-b phase shifter (360°/2^6).

The model is valid for a wide range of σ_A's and σ_β's as can be seen in Figs. 9 and 10, which show the effect of increasing variances σ_A and σ_β. Those figures were encountered utilizing the exact solution as described in [4]. Whereas an increasing σ_A scarcely has any effect, an increasing σ_β will somewhat increase ε_S. For σ_β< 30° the model underestimates the coefficient of variation by 10% or less.

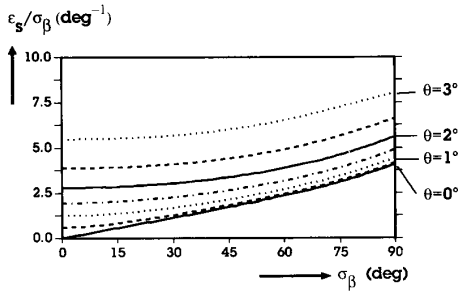

Fig. 10. The exact normalized coefficient of variation for θ=0, 1/2,..., 3° o=0 as a function of σ_β. For a 10% accuracy in ε_S at $\theta_{-3\,dB}$ = 2°, the phase variance must be smaller than σ_β<30°.

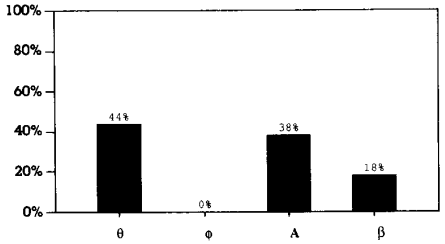

Fig. 11. Influence of the gain variables on the total error in the gain as a percentage.

The overall error bounds of the power density function can now be determined by substituting the worst-case values in (13):

$$\epsilon_G^2 \simeq \epsilon_S^2 = 0.73^2\,\sigma_\theta^2 + 0.025^2\sigma_\phi^2 + 0.187^2\sigma_A^2 + 0.00288^2\sigma_\beta^2. \tag{18}$$

In case of a digital system, the angle-error σ_θ can be utilized as a design parameter for the number of discrete amplitude- and phase values in the T/R-module, by requiring the contributions of the amplitude and phase errors to be smaller than the contribution of the angle error, σ_A < 0.73/0.187·σ_θ and σ_β < 0.73/0.00288·σ_θ.

The contributions of the amplitude and phase errors simply follow from the quantization error for which the variance in case of a linear binary system is given by:

$$\sigma^2 = \frac{1}{3}\left(\frac{U_{\max}}{2^q}\right)^2 \tag{19}$$

in which $U_{\max}$ is the maximum value and q is the number of bits.

If the antenna in the example is utilized in a motion compensated airborne radar (e.g., SAR) with a remaining stabilization error with σ_θ= 0.01°, the design requirements are met if the phase is tuned with $q_\beta \geq 6$ b, and the amplitude is tuned with $q_A \geq 4$ b, i.e., σ_A= 0.036 and σ_β =1.62°. Substitution of those values in (18) sets the total error bound at ε_S=1.11%.

Fig. 11 shows the individual influence of the four variables on the total error in the gain. Since the double summation in (15) is multiplied with $\sin\mu_\theta \ll 1$, and the variances of both angles can be expected to have the same magnitude $\sigma_\theta \approx \sigma_\phi$, the contribution of random ϕ-errors to ε_S is negligible as can be seen in Fig. 11.

VII. Conclusion

The calibration aspect of remote sensing radars has been discussed. A model which predicts the error bounds in a phased array antenna subject to random perturbations is described in this paper. As an example, the model is applied to a simple phased array antenna to explore the utility of the model. For a wide range of variances the model is in good agreement with the exact solution, but with a far less computer effort. Other, more complicated, antennas can be analyzed in a straightforward way. The model can be used as a design tool for digital phased array radar.

Acknowledgment

The work presented in this paper is a result of the calibration study into the project PHARUS (acronym for PHased ARray Universal SAR) [1]. The project PHARUS is carried out in a cooperation between the Physics and Electronics Laboratory of TNO (FEL-TNO), the National Aerospace Laboratory NLR, and the Delft University of Technology, Laboratory for Telecommunication and Remote Sensing Technology. The program management is carried out by the Netherlands Agency for Aerospace Programs (NIVR).

We would like to acknowledge the important contribution of L. Krul during the definition phase of the PHARUS project and with the preparation of this paper.

References

[1] P. Snoeij *et al.*, "The PHARUS airborne polarimetric C-band SAR project," *Proc. IGARSS '90*, Vol. 1, pp. 815–818, 1990.

[2] E. S. Kasischke and G. W. Fowler, "A statistical approach for determining radiometric precisions and accuracies in the calibration of synthetic aperture radar imagery," *IEEE Trans. Geosci. Remote Sensing*, vol. 27, July 1989.

[3] A. M. Breipohl, *Probabilistic Systems Analysis, an Introduction to Probabilistic Models, Decisions, and Applications of Random Processes.* New York: John Wiley & Sons, 1970.

[4] A. I. Zaghloul, "Statistical analysis of EIRP degradation in antenna arrays," *IEEE Trans. Antennas Propagat.*, vol. AP-33, pp. 217–221, Feb. 1985.

Paul Snoeij, for a photograph and biography, please see p. 735 of this issue of the TRANSACTIONS.

Arjen R. Vellekoop was born in Noordwykerhout on April 11, 1963. He received the M.Sc. degree in electrical engineering in 1989 from the Delft University of Technology, Delft, The Netherlands.